Lab on a Chip

RSC Publishing

PAPER

View Article Online
View Journal | View Issue

Cite this: *Lab Chip*, 2013, **13**, 4765

Synthesis of biomimetic oxygen-carrying compartmentalized microparticles using flow lithography†

Harry Z. An, Eric R. Safai, H. Burak Eral and Patrick S. Doyle*

Received 17th May 2013,
Accepted 27th September 2013

DOI: 10.1039/c3lc50610j

www.rsc.org/loc

We report a microfluidic approach for lithographically photo-patterning compartmentalized microparticles with any 2D-extruded shape, down to the cellular length scale (~10 microns). The prepolymer solution consists of a UV crosslinkable perfluorodecalin-in-water nanoemulsion stabilized by Pluronic® F-68. The nanoemulsions are generated using high-pressure homogenization and are osmotically stabilized by the trapped species method. The presence of PFC droplets increases the solubility and diffusivity of oxygen in the prepolymer solution, thereby enhancing the rate of O_2 inhibition during microparticle synthesis. We develop a simple model that successfully predicts the augmented O_2 mass transport, which agrees well with experimental data. Informed by our analytical results, cell-sized composite microgels are generated by controlling the oxygen environment around the polydimethylsiloxane (PDMS) microfluidic synthesis device. These nanoemulsion composites are functionally similar to red blood cells as oxygen carriers. Such bio-inspired polymeric particles with controlled physical properties are promising vehicles for drug delivery and clinical diagnostics.

Introduction

Bio-inspired polymeric particles are promising vehicles for drug delivery and clinical diagnostics.[1–3] These particles are synthetic constructs engineered in the likeness of natural particulates, such as pathogens and mammalian cells, and can mimic one or more key functions or attributes of their biological counterparts. A variety of top-down and bottom-up synthesis methods have been used, including self-assembly,[4] droplet microfluidics,[5] photolithography,[6,7] non-wetting template molding,[8] liquefaction and stretching,[9] and electrohydrodynamic jetting,[10] to manipulate the size, shape,[11] mechanical stiffness[12] and internal structure of these biomimetic microcarriers. The ability to precisely vary the particle physical properties is especially desirable as it allows these particles to maneuver through biological barriers, avoid cellular capture,[13] and even prolong circulation time[14] or alter biodistribution patterns *in vivo*. Therefore, versatile fabrication techniques that can provide independent control over critical particle design parameters are essential for modulating the interaction of these novel biomaterials with biological entities in biological environment.[15]

Currently, a facile technique for patterning morphologically complex, compartmentalized microparticles down to the cellular length scale (~10 microns) is still largely missing. Compartmentalization is one of the universal architectural motifs seen abundantly in eukaryotic cells, and allows a multitude of biochemical reactions to occur in perfect synchronicity in order to perform certain desired macroscopic cellular functions. Traditional methods of generating compartments in polymeric particles often suffer from 1) a lack of geometric complexity (due to surface tension forces, for example ref. 16) or 2) lower feature resolution.[17,18] The potential utility of multi-compartmental microparticles have already been demonstrated in several experiments: they can be used to efficiently co-encapsulate incompatible actives (*e.g.*, drugs, imaging modalities, *etc.*),[18,19] program delivery profiles and engineer different environmental release triggers (pH, temperature, light exposure, ultrasound, and external fields, *etc.*).[18,20–23]

Here, we show the reproducible synthesis of composite, biomimetic microparticles from crosslinkable oil-in-water nanoemulsions *via* a modified stop-flow lithography (SFL) technique. The dispersed phase consists predominantly of perfluorodecalin (PFD), the principal component in the first generation of perfluorocarbon (PFC)-based artificial blood products.[24] In general, PFCs are a class of biologically and chemically inert, highly hydrophobic, synthetic organic compounds. The inherent strength of the constituent C–F bonds, and therefore weak intermolecular forces, allow PFCs to efficiently solubilize respiratory gases (*i.e.*, O_2, CO_2). For example, the equilibrium partition coefficient, K, for O_2 between perfluorodecalin and water is ~O(10).[25] As such, PFCs are

Department of Chemical Engineering, Massachusetts Institute of Technology, Cambridge, MA, 02139, USA. E-mail: pdoyle@mit.edu

† Electronic supplementary information (ESI) available. See DOI: 10.1039/c3lc50610j

often used in artificial blood and cell culture[26] applications to enhance the rate of O_2 mass transfer.

Unlike our previous work involving silicone oil-based nanoemulsions, the PFD-based formulations are biocompatible but require further stabilization due to a finite solubility of oil in the aqueous continuous phase.[21] The PFC-laden composite microgels are structurally and functionally reminiscent of erythrocytes, which are long-circulating biological entities responsible for oxygen delivery *in vivo*. Fabrication of these PFC solutions is challenging as they facilitate oxygen transport, which in turn inhibits free radical polymerization, and impedes bulk gelation. To generate these biomimetic, oxygen-carrying composite microparticles, we take a rational engineering approach to first slow the coarsening of the PFC nanoemulsion through variation in composition, and then lower the effective concentration of oxygen, a common radical scavenger during synthesis, using a purge chamber filled with an inert gas. This synthesis technique allows cell-sized, shape-anisotropic microparticles to be patterned in a semi-continuous fashion. One of the key advantages of this process is that the properties of the carrier particle and those of the encapsulated compartments can be optimized separately for a diverse set of biomedical applications.

Materials and methods

Materials and nanoemulsion preparation

The crosslinkable oil-in-water nanoemulsions used in this work contain perfluorinated oils: perfluorodecalin and perfluorotripropylamine (Oakwood Chemicals, Inc.) dispersed in an aqueous phase consisting of poly(ethylene glycol) diacrylate (PEGDA, M_n = 700 g mol^{-1}) and non-ionic surfactant Pluronic® F-68 (PF68). Additives included the photoinitiator 2-hydroxy-2-methyl-1-phenyl-propan-1-one (Darocur® 1173) and the lipophilic dye, PKH26 ($\lambda_{ex}/\lambda_{em}$ = 551/567 nm, Invitrogen) in ethanol. The latter was used to label the encapsulated oil nanodroplets for fluorescent imaging. Unless otherwise noted, all materials were obtained from Sigma Aldrich and used as supplied.

To prepare the nanoemulsions, a crude pre-emulsion was first generated as previously described[21] by adding the perfluorinated oil(s) drop-wise to an aqueous continuous phase containing 36% (v/v) PEGDA and 2–40 mM PF68 under constant agitation using a magnetic stirrer. The corresponding nanoemulsion was then created by high pressure homogenization (EmulsiFlex-C3, AVESTIN) at 5–20 kpsi for up to 20 passes. Prior to composite particle synthesis, 4% (v/v) Darocur® 1173 and 10 μM PKH26 (if necessary for imaging purposes) were added to aliquots of the nanoemulsion, followed by vortex mixing.

Particle synthesis

All of the particles shown in this work were prepared using a modified stop-flow lithography (SFL) technique in rectangular microfluidic channels (PDMS, Sylgard 184, Dow Corning). Channel heights ranged from 20 to 50 μm. The synthesis devices were placed inside a custom-made sealed chamber with an inert gas purge inlet. Briefly, the prepolymer mixture (degassed for 60 minutes under gentle argon flow, unless otherwise specified) was injected into a synthesis device using modified pipette tips (Molecular BioProducts) as delivery chambers under moderate forcing pressure (~3 psi). Cell-like composite microparticles were patterned by projecting mask-defined UV light from a Lumen 200 metal arc lamp (Prior Scientific) through a wide excitation UV filter set (11000v2 UV, Chroma Technology). A shutter system (VS25, Uniblitz) interfaced with a custom-written Python automation script precisely controlled the duration of UV exposure, which typically ranged from 150 to 800 ms depending on particle shape and size. Microparticle formation was visualized using a cooled interline charge-coupled device camera (Clara, Andor).

Following polymerization, particles were transferred from the outlet reservoir of the microfluidic synthesis device to a clean 1.5 mL Eppendorf tube containing 600 μL PBST (1× phosphate buffered saline with 0.1% (v/v) Tween® 20). Particles were washed and re-suspended four times in PBST then stored at room temperature for imaging.

Nanoemulsion characterization

Nanoemulsion droplet sizes were measured *via* dynamic light scattering using a Brookhaven Instruments BI-200SM multi-angle apparatus. Samples were diluted to φ = 0.0005 using a mixture of 33% PEGDA700 in deionized water. Autocorrelation functions were measured at a scattering angle of 90° and a temperature of 25 °C. A cumulant analysis was conducted on the data acquired to obtain the hydrodynamic droplet diameter 2*R*. Coefficient of variation (C.V.) is defined here as the variance of the size distribution relative to the mean size.

Microparticle characterization

PKH26-labeled composite microparticles were harvested from the synthesis devices and stored in 1X PBS buffer containing 0.1% Tween 20 prior to imaging using a laser confocal scanning microscope (Zeiss LSM Meta 510) equipped with an argon laser (543 nm). Successive *x*–*y* scans were acquired at intervals of 0.1 μm in the *z*-direction through representative particles using a 100× oil objective. The images were analyzed using ImageJ (NIH).

Perfluorodecalin/water surface tension measurements were taken using the pendant droplet method on a DSA 10 tensiometer (Kruss). A calibration curve was prepared by measuring surface tension for a set of Pluronic® F-68 standard solutions at room temperature.

Results and discussion

To synthesize RBC-like microparticles (Fig. 1), we use an oil-in-water (O/W) nanoemulsion composed of perfluorodecalin oil (MW = 462 g mol^{-1}) stabilized by Pluronic® F-68, dispersed in an aqueous continuous phase containing 36% poly(ethylene glycol) diacrylate (PEGDA, M_n = 700 g mol^{-1}) and 4% Darocur® 1173. PEGDA and Darocur act as the crosslinker and photoinitiator, respectively. During UV exposure, Darocur

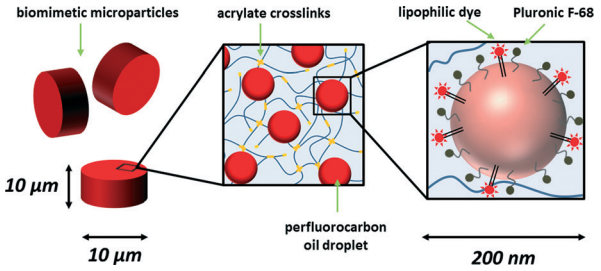

Fig. 1 Schematic depiction of biomimetic composite microparticles. Stop-flow lithography reproducibly generates these microparticles from UV-crosslinkable perfluorocarbon oil-in-water nanoemulsions. The nanometer-sized oil droplets contain a mixture of perfluorodecalin and perfluorotripropylamine, stabilized by a biocompatible nonionic surfactant, Pluronic® F-68. The droplets are kinetically arrested within the gel network, as indicated by lipophilic dye labeling, and can facilitate oxygen transport, similar to red blood cells.

undergoes photolysis and initiates polymerization of the acrylate end-groups on the PEGDA molecules. This results in the formation of a crosslinked hydrogel network that kinetically traps the perfluorocarbon oil droplets.

Nanoemulsion formulation and stability

The crosslinkable O/W nanoemulsions are generated *via* a two-step emulsification process. In the first step, a pre-mix macroemulsion is generated using a magnetic stirring device, fixing the emulsion composition. Next, the pre-mix is transferred to a high-pressure homogenizer and forced through an adjustable homogenizing valve at elevated pressures (≤20 kpsi), during which droplets experience the elongational stress needed to overcome the significant Laplace pressure difference and to rupture down to the nanometer size scale.[27] It is worth noting that in the emulsion literature, there lacks a universally-accepted cut-off below which a colloidal dispersion would be considered a nanoemulsion. Here, we define a nanoemulsion as a metastable suspension consisting of two incompatible phases, with the dispersed phase having diameter below 200 nm.[27]

To assess the stability of the PFC nanoemulsions over time, we prepared an 8% (v/v) perfluorodecalin-in-water nanoemulsion containing 40 mM Pluronic® F-68, and 36% PEGDA700 (φ = 0.08, C_s = 42 mM, P = 0.36). The nanoemulsion is homogenized at 20 kpsi for 10 passes. The as-prepared sample has an initial droplet diameter of ~167 nm. A time course of the droplet volume growth at 4 °C was tracked *via* DLS and shown in Fig. 2A. As expected, due to their nanoscopic size and non-zero coefficient of variation (defined here as the variance in droplet size over the mean), the droplets mainly coarsen *via* the Ostwald ripening mechanism, according to

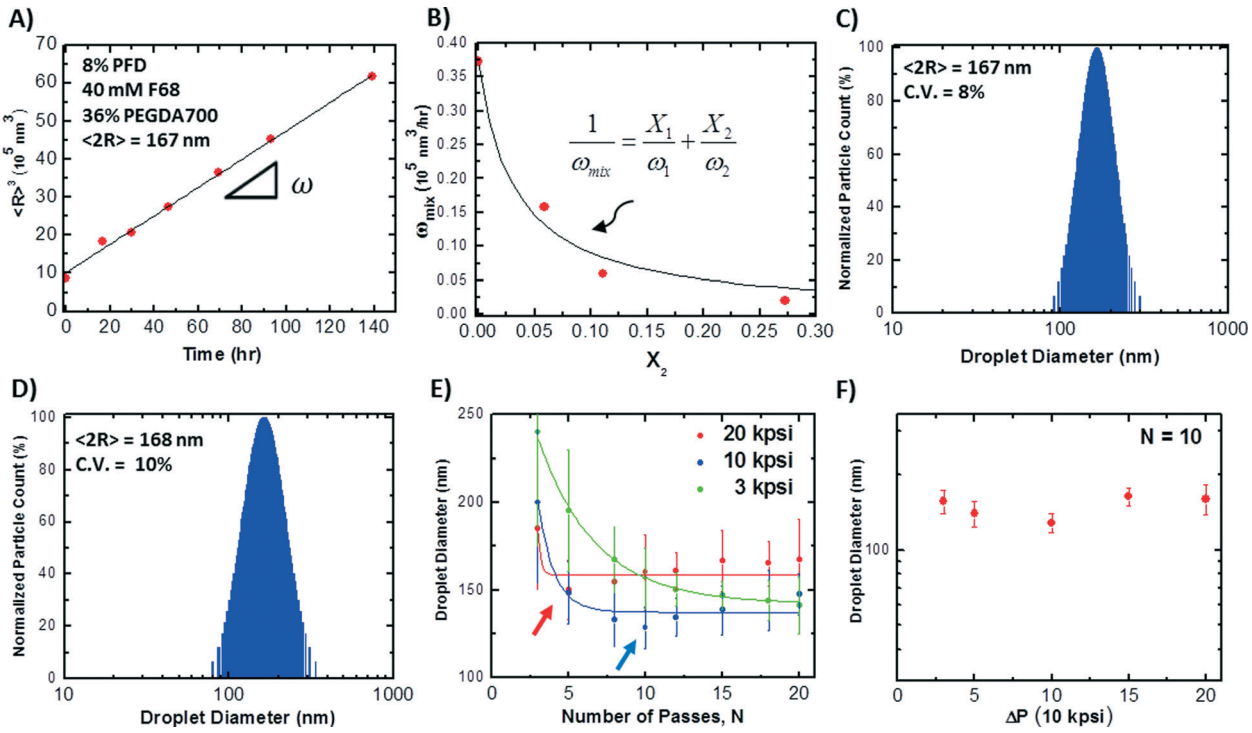

Fig. 2 Nanoemulsion formation and stability. (A) Time evolution of average droplet volume for an 8% v/v perfluorodecalin (PFD)-in-water nanoemulsion containing 36% poly(ethylene glycol) diacrylate (M_n = 700 g mol^{-1}) and stabilized by 40 mM PF68. The initial droplet is 167 nm. The linear trend observed suggests that the dominant coarsening mechanism is Ostwald ripening, with characteristic rate ω. (B) Variation of ω with the addition of a high molecular weight 'trapped species' perfluorotripropylamine (PFTPA), which can counteract Ostwald ripening by creating an entropic barrier for de-mixing. The solid line shows theoretical prediction using eqn (2). Normalized droplet size distributions were measured using dynamic light scattering for 8% perfluorodecalin-in-water nanoemulsions (P = 0.36 PEGDA, C_s = 40 mM) containing (C) 0% v/v PFTPA and (D) 0.5% v/v PFTPA. The nanoemulsion samples were prepared using high-pressure homogenization at 20 kpsi for 10 passes. Addition of the oil stabilizer has minimal impact on the initial droplet diameter and monodispersity (upper-left corner). (E) The evolution of average droplet diameter with the number of passes, N, through the homogenization device for an 8% PFD-in-water nanoemulsion (φ_2 = 0.005, P = 0.36 PEGDA, C_s = 40 mM) at three different pressures. Lines give fit to the exponential relationship suggested by Mason *et al.* [ref. 33]. (F) The evolution of average droplet diameter with homogenization pressure for N = 10.

$\langle R\rangle^3 \sim \omega t$. Ostwald ripening is a process driven by molecular diffusion, whereby larger droplets grow at the expense of smaller ones in order to minimize the total interfacial area.[28] ω is the ripening rate, and can be analytically expressed as:[29]

$$\omega = \frac{8\nu^2 D_{oil} C_\infty \gamma}{9RT} \quad (1)$$

where ν, D_{oil}, and C_∞ are the molar volume, diffusion coefficient, and bulk solubility of oil through the continuous phase, respectively. γ is the surface tension, R is the universal gas constant, and T is the absolute temperature. The measured ripening rate (~600 $nm^3\ min^{-1}$) is much higher than that of the silicone oil formulations (~0.1 $nm^3\ min^{-1}$) we had previously studied, due to a finite solubility of perfluorodecalin in the aqueous continuous phase.[21,30]

To improve the stability of nanoemulsion prepolymer and to lengthen its shelf-life for particle synthesis, we added minor amounts (≤3% by volume) of perfluorotripropylamine (PFTPA) into an 8% perfluorodecalin nanoemulsion. PFTPA is an insoluble oil species with a moderate *in vivo* retention time of ~60 days, short in comparison to other commercially-available perfluorinated compounds with similar molecular weights (521 g mol^{-1}).[24] PFTPA preferentially partitions to the oil droplet interior and exerts an osmotic pressure that counterbalances the forces that cause Ostwald ripening.[31] Initial repartitioning of the mobile oil component between droplets due to Ostwald ripening creates an entropic barrier that retards further oil de-mixing. As shown in Fig. 2B, ω decreases asymptotically with PFTPA addition. The overall growth trend is well predicted by the following mixing law:[32]

$$\omega_{mix} = \left(\frac{X_1}{\omega_1} + \frac{X_2}{\omega_2}\right)^{-1} \quad (2)$$

where X_1 and X_2 are the oil-based volume fractions of PFD and PFTPA, respectively. The ripening rate for a pure PFTPA nanoemulsion, ω_2, is approximated using previously reported values of aqueous bulk solubility (Table 1) according to:

$$\omega_2 \approx \omega_1 \frac{C_{\infty,2}}{C_{\infty,1}} \quad (3)$$

Addition of the 'trapped species' has little effect on droplet size or coefficient of variation, as indicated by the similar droplet size distributions measured for two batches of 8% PFD-in-water nanoemulsions with 0% PFTPA (Fig. 2C) and 0.5% PFTPA by volume (Fig. 2D) prepared at 20 kpsi (N = 10).

To further demonstrate the instability of PFC nanoemulsions, we note the evolution in droplet size as a function of the number of passes, N, for a range of homogenization pressures (3–20 kpsi). Typically, we use the number of passes through the homogenizing device to tune the droplet polydispersity.[21] This is because the flow field near the homogenizing valve is highly nonhomogeneous and turbulent. Passing an emulsion sample through the device repeatedly allows droplets to experience similar strain histories, and lowers droplet polydispersity. Similarly, over time, the average droplet size tends to exponentially approach a final saturation value.[33] In the case of PFC nanoemulsions, however, the droplet size trajectory passes through a minimum when pressures ≥10 kpsi (Fig. 2E, red and blue arrows) and then slightly increases with N. Within this pressure regime, the $<2R>$ *vs.* N trends are poorly described by the exponential relationship proposed by Mason and coworkers.[33] This suggests that the droplets may be undergoing re-coalescence during homogenization as it is difficult for off-the-shelf surfactants, such as Pluronic® F-68, to effectively stabilize newly created O/W interfaces during droplet collisions. The re-coalescence behavior is further evidenced by the weak power-law dependence of droplet size on homogenization pressure ($D \propto \Delta P^{0.03}$, Fig. 2F).

Table 1 Summary of reported aqueous bulk solubilities of PFD (component 1) and PFTPA (component 2) and estimated ripening rates of the corresponding crosslinkable PFC-in-water nanoemulsions

Parameter	Value	Units	Source
$C_{\infty,1}$	99	10^{-10} M	Ref. 29
$C_{\infty,2}$	2.8	10^{-10} M	Ref. 29
ω_1	37.2	$10^3\ nm^3\ h^{-1}$	Measured
ω_2	1.1	$10^3\ nm^3\ h^{-1}$	Calculated

PFC-laden composite particle synthesis

To synthesize cell-like microparticles, we use the canonical prepolymer formulation containing 8% PFD, 0.5% PFTPA (by volume) dispersed in an aqueous continuous phase of 36% PEGDA700, 20 mM Pluronic® F-68 and 4% photoinitiator (Darocur). Adjusting the surfactant concentration from 2 to 40 mM does not improve emulsion stability against ripening due to negligible changes in surface tension over this concentration regime. The oil volume fraction can be arbitrarily lowered without causing droplet coalescence by diluting a concentrated emulsion stock with pure continuous phase containing the same concentration of PF68 (ESI†).

The high oxygen content of PFC-laden prepolymer solution is counterproductive towards particle photo-patterning *via* stop-flow lithography (SFL).[6,34] In traditional SFL, pulses of mask-defined UV light are projected through a microscope objective to generate free-standing gel structures within a microfluidic device, down to the micron-scale (Fig. 3A). The ability to generate free-standing microparticles of potentially any 2D-extruded shape is intimately tied to oxygen transport; during particle synthesis, oxygen, a radical scavenger, rapidly diffuses through the porous walls of the polydimethylsiloxane (PDMS) device and inhibits the UV-initiated polymerization by reacting with propagating oligomers, forming chain-terminating peroxide species (Fig. 3A, right).[34] Typically, the level of O_2 must be reduced by at least three orders of magnitude before bulk gelation can occur.[34] Where the rate of oxygen diffusion balances that of oxygen inhibition near the channel periphery, lubricating layers of unpolymerized material, termed

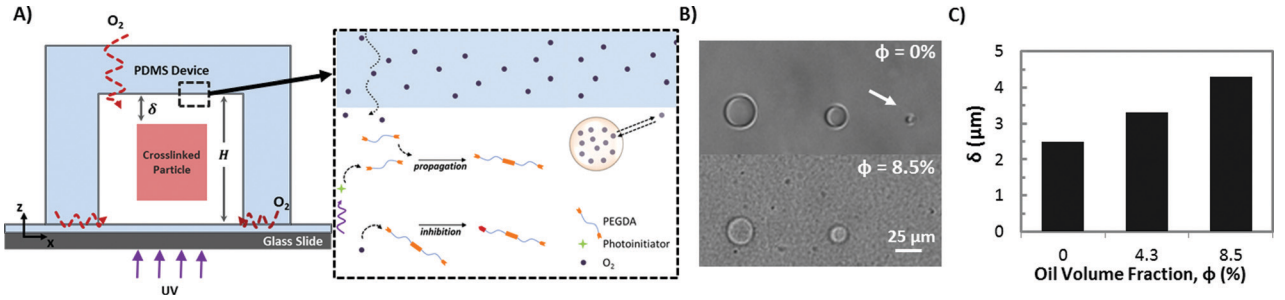

Fig. 3 Effect of oxygen on photo-polymerization. (A) Schematic of the cross-sectional view of a PDMS synthesis device showing the formation of a disc-shaped composite particle using stop-flow lithography. The particle is flanked on either side by films with thickness δ of unpolymerized oligomers (left). O_2 rapidly diffuses through the PDMS side walls and partitions into the perfluorocarbon oil droplets (right). During polymerization, O_2 consumption in the continuous phase *via* inhibition reactions with propagating PEG oligomers leads to further O_2 release from the oil droplets. (B) Micrographs of a series of discs with decreasing feature size polymerized in a 15 μm tall device using prepolymers composed of 0% PFC (P = 0.36 PEGDA, PI = 0.04) and 8.5% PFC (φ_1 = 0.08, φ_2 = 0.005, C_s = 20 mM). The composite microparticles are consistently under-polymerized due to an increased effective O_2 concentration in the presence of PFC nanodroplets. (C) Inhibition layer thickness, δ, grows with PFC content showing quantitative evidence for facilitated transport of O_2.

the inhibition layer, form above and below the crosslinked particles, and allow them to be advected downstream for collection. As the inhibition layer thickness (δ) approaches the channel height, as it does in the case of generating cell-sized composites, particle synthesis becomes proportionally more difficult. Using a one-dimensional reaction–diffusion model for photopolymerization within a PDMS microfluidic device, Dendukuri *et al.*[34] previously derived analytical scaling relationships for δ and τ (the time required to deplete the oxygen present and trigger crosslinking) and showed that both are inversely related to a Damköhler number, Da, which denotes the competition between the rate of oxygen inhibition to the rate of oxygen diffusion into the prepolymer:

$$\mathrm{Da} = \frac{\psi\varepsilon I_0[\mathrm{PI}]H^2}{D[\mathrm{O_2}]} \tag{4}$$

where Ψ is the quantum yield of formation of the initiating radicals, [PI] and ε are the photoinitiator concentration and molar extinction coefficient, respectively, I_0 is the incident intensity of UV light, H is the channel height, D is the oxygen diffusivity, and $[O_2]$ is the oxygen concentration in the prepolymer. The use of PFCs in the prepolymer lowers the achievable feature resolution under similar exposure conditions, as compared to a pure PEGDA-based prepolymer, by increasing both the diffusivity and solubility of O_2.

To demonstrate this qualitatively, we polymerized a series of discs of varying diameters ranging from 15 to 25 μm in a 20 μm tall PDMS device. Two types of prepolymers were used, only one of which contained the nominal 8.5% perfluorocarbon oil, the other containing none. Using the same exposure duration (800 ms) and intensity, all of the disks formed in the nanoemulsion prepolymer stream were under-polymerized (Fig. 3B); whereas the two largest discs fully polymerized in the PFC-free prepolymer. This was because PFC nanodroplets acted as point sources of oxygen and released O_2 almost instantaneously during UV exposure. As a result, the induction time increased, and the onset of bulk gelation was delayed.

To quantitatively evaluate the effect of the presence of PFC on the efficacy of particle patterning, we look at the channel cross-section (z-direction), and compare the inhibition layer thickness in the presence and absence of PFCs in the prepolymer solution.[34] It has been previously shown that $\delta \sim \mathrm{Da}^{-1/2}$. Therefore, using similar polymerization conditions, the ratio of the two δ's – with and without PFCs – simplifies to:

$$\frac{\delta}{\delta_0} = \sqrt{\frac{D[\mathrm{O_2}]}{D_0[\mathrm{O_2}]_0}} \tag{5}$$

Here, the 'zero' subscript indicates the continuous phase (*i.e.*, in the absence of PFCs). The ratio of the equilibrium oxygen concentrations can be estimated based on a simple volume-average:

$$[\mathrm{O_2}] = (1-\varphi)[\mathrm{O_2}]_0 + \varphi[\mathrm{O_2}]_{\mathrm{PFC}} \tag{6}$$

eqn (6) can be re-written by eliminating $[O_2]_{PFC}$ using the partition coefficient, $K = [O_2]_{PFC}/[O_2]_0$:

$$\frac{[\mathrm{O_2}]}{[\mathrm{O_2}]_0} = 1 + (K-1)\varphi \tag{7}$$

Substituting K = 16, a 8.5% by volume PFC nanoemulsion, the RHS of eqn (7) equals ~2.2,[25] indicating a higher overall concentration of oxygen, though only oxygen present in the continuous phase can participate in the inhibition reaction.

Next, we derive a mean-field analytical expression for the effective oxygen diffusion coefficient, D, in the presence of PFC droplets. Here, for simplicity, we treat the emulsion prepolymer as a homogenous material, with D as the characteristic oxygen diffusivity that must be used to describe the mass transfer occurring on a length scale much greater than the average spacing between droplets. D is found by considering the far-field perturbation in the oxygen concentration field caused by the PFC oil droplets. A similar mean-field

approach was taken by Deen to derive the effective conductivity of a particle suspension.[35]

We model the nanoemulsion as a dilute suspension of spherical particles with a uniform number density of n, occupying a spherical volume of radius a sufficiently large to contain many particles. Far from this volume, the total oxygen concentration perturbation at r due to the oil droplet is:

$$C_p^{total}(r) = \frac{4\pi}{3} a^3 n C_p(r) \quad (8)$$

C_p represents the single-particle contribution derived from solving for the oxygen concentration field in a simple system consisting of a spherical particle (*e.g.*, a PFC droplet) of radius R surrounded by a different material (*e.g.*, the aqueous continuous phase). The droplet and the continuous phase have different oxygen diffusion coefficients, D_{PFC} and D_0, respectively. A constant mass flux, G , parallel to the z-axis (Fig. 3A) is assumed far from the sphere due to an imposed oxygen concentration gradient resulting from particle polymerization. The steady-state oxygen concentration outside the droplet, $\Psi(r, \eta)$, is governed by mass conservation:

$$\frac{\partial}{\partial r}\left(r^2 \frac{\partial \psi}{\partial r}\right) + \frac{\partial}{\partial \eta}\left((1-\eta^2)\frac{\partial \psi}{\partial \eta}\right) = 0 \quad (9)$$

$$\frac{\partial \psi}{\partial z}(\infty, \eta) = G \quad (10)$$

Similarly, the concentration within the sphere, $\Lambda(r, \eta)$ is given by:

$$\frac{\partial}{\partial r}\left(r^2 \frac{\partial \Lambda}{\partial r}\right) + \frac{\partial}{\partial \eta}\left((1-\eta^2)\frac{\partial \Lambda}{\partial \eta}\right) = 0 \quad (11)$$

with a finite concentration at the center of the droplet. The two governing equations are coupled by the matching concentration and flux boundary conditions at the oil/water-PEGDA interface.

$$\Lambda(R, \eta) = K\psi(R, \eta) \quad (12)$$

$$D_{PFC} \frac{\partial}{\partial r}\Lambda(R, \eta) = D_0 \frac{\partial}{\partial r}\psi(R, \eta) \quad (13)$$

This system of coupled PDEs can be solved using Legendre polynomials and the finite Fourier transform method. The full solution appears in the ESI.† The O_2 concentration field outside the droplet is:

$$\psi(r, \eta) = A + Gr\eta + \left(\frac{1-\beta}{2+\beta}\right)\frac{R^3}{r^3} Gr\eta \quad (14)$$

with $\beta = D_{PFC}/D_0$ and A an arbitrary constant, undetermined due to the Neumann boundary condition imposed at $r = \infty$. From the final solution for the concentration field, it is seen that the effect of the droplet on the continuous phase oxygen concentration decays as r^{-2}. Equating the last term on the RHS of eqn (14) to C_p, and inserting it into eqn (8):

$$C_p^{total}(r) = \varphi a^3 \left(\frac{1-\beta}{2+\beta}\right)\left(\frac{G\eta}{r^2}\right) \quad (15)$$

where φ is the droplet volume fraction.

Finally, the effective diffusivity of oxygen in the nanoemulsion is found by comparing eqn (15) with the case of a homogenous material characterized by diffusivity parameter, $\beta' = D/D_0$, occupying the same volume, *i.e.*, setting $R = a$ in eqn (14) and writing a second equivalent expression for C_p^{total} and solving for D:

$$D = D_0\left(1 + 3\left(\frac{\beta - 1}{\beta + 2}\right)\varphi + O(\varphi^2)\right) \quad (16)$$

This is analogous to the result derived for the conductivity of a particle suspension.[36,35] If we neglect any particle–particle interactions (*e.g.*, in the dilute regime), it is seen that the first correction to the diffusion coefficient is proportional to the oil volume fraction. Substituting representative values for D_{PFC} (1.88×10^{-8} m^2 s^{-1})[37] and D_0 (2.84×10^{-11} m^2 s^{-1})[34] into eqn (16) for a 8.5% emulsion, D/D_0 is approximately equal to 1.3. Evaluating eqn (5) using eqn (7) and (16) gives theoretical predictions for δ/δ_0 for various oil volume fractions.

To compare the theoretical prediction with experimental data, we synthesized disc-shaped particles containing 0%, 4.3% and 8.5% PFC emulsion (C_s = 20 mM) in a 50 μm tall device and estimated the inhibition layer thickness, δ, from the corresponding particle height measurements (Fig. 3C). δ is assumed to be symmetric with respect to the channel center. The experimental estimates agree with model predictions to within 0.1 μm. It is seen that δ grows with φ, as a result of 1) faster O_2 transport and 2) greater O_2 solubility. The latter contribution is stronger, especially at higher oil volume fractions. In a PFC emulsion solution, oxygen can exist and freely diffuse between two different chemical environments, thereby increasing the overall effective concentration that must be overcome during synthesis in order to reproducibly generate composite microparticles.

One of the practical implications of the theoretical analysis presented above is that to achieve particle feature resolution on par with the cellular length scale (~10 μm), one must overcome the engineering challenge of controlling the oxygen environment in the immediate vicinity of the microfluidic device during particle synthesis. We note that other more direct methods of expediting polymerization kinetics, such as adding in more photoinitiator or crosslinker, result in droplet aggregation (ESI†).

To demonstrate that we can generate RBC-like, 10 μm composite particles, we placed a synthesis device in a custom-made purge chamber. Use of the chamber afforded two distinct advantages: 1) it allowed particles to be patterned in a more controlled fashion, according to the *size and shape* of the lithographic photomask, and 2) it enabled us to alter the O_2 concentration using an inert gas (*e.g.*, argon). Oxygen concentration is a crucial control parameter during the synthesis of cell-sized, geometrically-complex features (non-circular, or with internal cavities, for example). The modified SFL setup is shown schematically in Fig. 4A. The chamber was loosely sealed with side inlets for introducing argon and/or air. We degassed an 8.5% PFC emulsion prepolymer by slowly bubbling argon for 60 minutes prior to flowing it into the microchannel. This pre-synthesis treatment step lowered the oxygen concentration, and improved the particle resolution (Fig. 4C, i), though the disc-shaped particles remain underpolymerized, in the in-plane and out-of-plane (height) dimensions. To decrease $[O_2]$ further, we performed particle synthesis within the purge chamber under gentle influx (~1 psi) of argon. By polymerizing the same sequence of circles (Fig. 4B, right) using identical exposure conditions (800 ms) at discrete time points, we show that 10 μm (diameter) × 10 μm (height) composite microparticles can be made after 50 minutes of Ar purge (Fig. 4C, iii, white arrow). This timescale was dictated by the diffusion of argon through the PDMS device. To emphasize the deleterious effects of O_2 on polymerization kinetics, we let the PDMS device re-saturate with oxygen. ~40 minutes after the removal of the purge chamber (Fig. 4C, iv), the achievable feature resolution returned to the pre-purge state, again showing the inhibitory effects of oxygen.

Interestingly, controlling the amount of oxygen present during particle synthesis presents a simple method to fabricate particles of different heights *within the same channel* without resorting to sheath flows above and below the prepolymer stream. To show this, we quantified the change of inhibition layer thickness as a function of the surrounding oxygen partial pressure in the purge chamber. The oxygen partial pressure was manipulated by controlling the inlet pressures of two purge gas streams: air (21% O_2) and argon (0% O_2). After the synthesis microfluidic device equilibrated with the surrounding gas mixture, we fabricated 25 μm (side) squares in a 30 μm tall device. To measure the inhibition layer thickness, we toppled the particles by temporarily applying a sharp pressure pulse (~1 s), which caused them to fall onto their sides. The results are shown in Fig. 5. As the concentration of oxygen decreases, δ decreases sharply. Furthermore, we recover the known scaling, $\delta^2 \sim [O_2]$, derived previously by Dendukuri *et al.*[34]

Composite particle analysis

A fluorescent micrograph of a typical collection of 10 μm (diameter) by 10 μm (height) PFC nanoemulsion composites is shown in Fig. 6A. We made these particles in a 20 μm-tall device using a degassed, PKH26-labeled prepolymer (10 μM) in the purge chamber, after ~60 minutes of Ar flow. PKH26 is a lipophilic dye that readily partitions to the droplet interface. Based on dimensions of the purge chamber (0.1 m × 0.1 m × 0.05 m), and an estimated Ar flow rate of ~10^{-3} m^3 s^{-1} under well-mixed conditions, the purging step reduced the oxygen concentration in the head space above the microfluidic device by ~10^4-fold. During synthesis, we turned off the purge stream to maintain the gas environment at pseudo-steady state. Excessive argon purge caused particles to adhere to the PDMS device due to the complete lack of O_2 inhibition. Photoluminescence analysis on individual particles indicated uniform droplet loading (Fig. 6B). We can also synthesize particles of other 2D-extruded shapes by using different

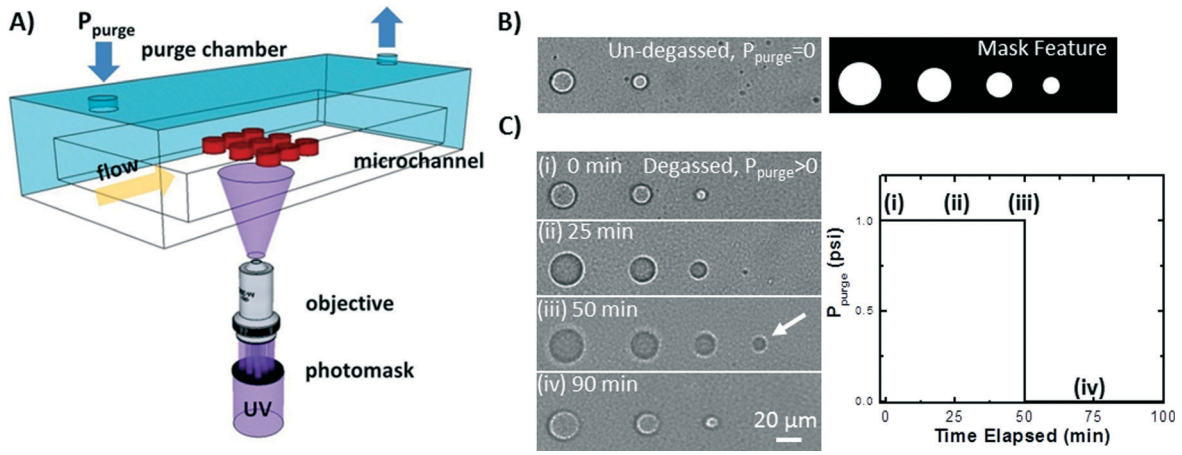

Fig. 4 Stop-flow lithography (SFL) experimental setup. (A) Schematic drawing showing the formation of an array of biomimetic composite disc-shaped particles using SFL. A prepolymer containing crosslinkable PFC-in-water nanoemulsions is flowed through a PDMS synthesis device and polymerized *via* controlled pulses of mask-defined UV light through a microscope objective. The gel particles are then advected downstream for collection. The synthesis device is enclosed in a custom-made purge chamber, which allows the exchange of an inert gas. Micrographs showing the polymerization of a series of circular mask features (B, right) in nanoemulsion prepolymer stream (φ_1 = 0.08, φ_2 = 0.005, C_s = 20 mM, *P* = 0.36 PEGDA, PI = 0.04) that is (B, left) un-degassed, at ambient conditions (no purge chamber), and (C) degassed for 60 min, and in the purge chamber under a constant influx of argon. The particle in-plane feature resolution improves over time. (iii) The 10 μm feature (white arrow) fully polymerizes after 50 min of Ar flow. (iv) 40 min after Ar flow has been turned off, the feature resolution returns to the initial configuration.

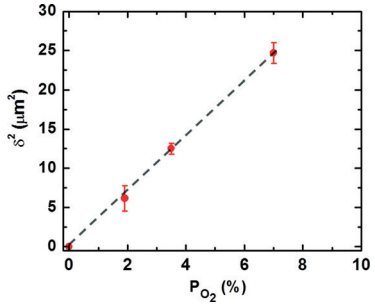

Fig. 5 Variation of inhibition layer thickness, δ, with oxygen partial pressure (P_{O2}). The linear trend observed in the δ^2 *vs.* P_{O2} space agrees well with the known scaling relationship eqn (5) discussed previously. A dash line is drawn to guide the eye.

photomasks. A triangle-shaped particle (φ_1 = 0.08, φ_2 = 0.005) is shown in Fig. S4 (ESI†).

To ascertain that oil droplets did not undergo aggregation during particle synthesis, we synthesized 20 μm (diameter) by 10 μm (height) disks using a prepolymer containing 0.01% by volume nanoemulsion. The low oil volume fraction allowed us to distinguish individual emulsion droplets. Confocal images of higher volume fraction particles are given in ESI.† The oil volume fraction was lowered by diluting the canonical prepolymer formulation using pure continuous phase without altering the bulk surfactant concentration. At such a low φ, using a 100× oil objective and imaging z slices at 100 nm intervals, we observed droplets randomly dispersed throughout the particle, kinetically arrested by the gel network. Two representative orthogonal optical sections are shown in Fig. 7. Furthermore, the volume fraction of encapsulated droplets matched that which was originally present in the prepolymer solution. In this analysis, we first identified the number of droplets in confocal z scans manually using ImageJ (see ESI† for a detailed discussion). We then estimated the volume fraction of the encapsulated droplets by using the initial average droplet diameter (197 nm) in the prepolymer solution, an estimated depth of focus (1.6 μm), and the diameter (20 μm) of the composite gel particle. The encapsulated oil volume fraction was found to be ~0.012% or 20% greater than φ in the prepolymer. This result is within the uncertainty of our measurement due to the polydispersity of the droplets. This suggests that the droplet loading remained unaffected by polymerization.

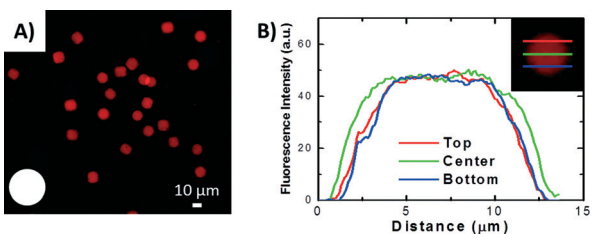

Fig. 6 Biomimetic nanoemulsion composites. (A) Fluorescent micrograph of 10 μm (diameter) by 10 μm (height) disc-shaped particles pre-loaded with PKH26. The transparency mask feature used during synthesis is shown in the lower inset. (B) Spatially resolved fluorescence intensity profiles (a.u. = arbitrary units) taken across three different lanes of the particle shown in the upper inset.

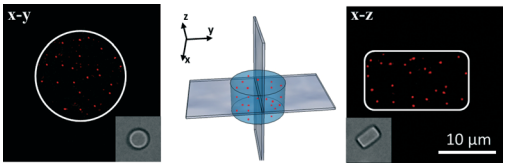

Fig. 7 Laser confocal images (left: x–y plane, right: x–z plane) of a 20 μm (diameter) × 10 μm (height) disc-shaped composite particle (φ =0.0001, C_s = 20 mM, P = 0.36 PEGDA700, PI =0.04) showing even dispersion of PKH26-labeled PFC nanodroplets. (Insets) The corresponding cross-sectional bright-field images. Schematic (center panel) marks the approximate locations of the representative confocal slices.

Finally, encapsulating PFC nanodroplets in the hydrogel network allows us to arbitrarily tune the bulk surfactant concentration by simple washing steps post-synthesis. Excess surfactant, orders of magnitude greater than the critical micelle concentration (CMC), is required to minimize the final droplet size by 1) lowering the surface free energy, and 2) stabilizing newly formed droplets against shear-induced coalescence during homogenization. However, for many cellular assays, having such a high concentration of surfactant is undesirable, as it may compromise membrane integrity and result in cell lysis and protein denaturation.[38] Studies have also shown that surfactants may cause skin irritation,[39] or trigger immune responses (*i.e.*, complement activation, anaphylactic-type reactions) *in vivo*, at low test doses.[40] Kinetically arresting the droplets in gel particles allows us to use centrifugation to quickly sediment the nanoemulsion composites and replace the surfactant-rich supernatant with pure buffer. To demonstrate this, we measured the surface tension of the displaced supernatant solution after a number of rinsing steps using the pendant drop method, and estimated the corresponding PF68 concentration from a calibration curve (Fig. S1†). As seen in Fig. 8, the surfactant concentration decreased by ~4 logs after 4 short (2-minute) rinse cycles. The washing procedure had a negligible effect on the stability of the encapsulated droplets (Fig. 7). We emphasize that it is not possible to generate small

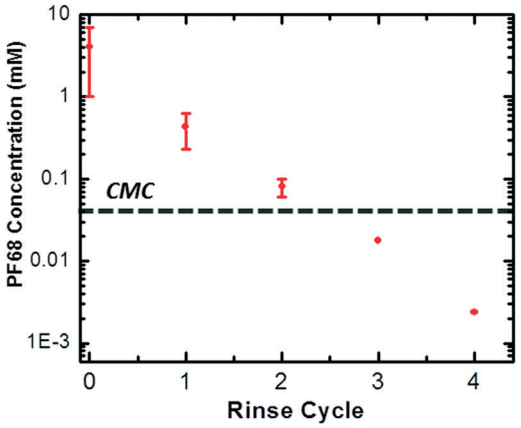

Fig. 8 Concentration of Pluronic® F-68 (PF68) in the supernatant of particle storage solutions as a function of the number of rinse cycles. The dashed line indicates the experimentally determined critical micelle concentration (CMC) for PF68 in water at room temperature.

droplets ($2R$ ~ 200 nm) under nearly surfactant-free conditions *a priori* due to surface tension effects.

Conclusions

In summary, we presented a versatile microfluidic approach for photopatterning PFC-laden nanoemulsion composites with resolution down to the cellular length scale (~10 μm). The PFC droplets are randomly distributed throughout the gel interior. We proposed a simple steady-state two-phase diffusion model to successfully predict the accelerated rate of O_2 mass transport in the presence of PFC nanodroplets. To minimize the impact of excess oxygen on polymerization, an enclosed chamber with a purge gas inlet was used to control the oxygen environment around the PDMS synthesis device.

The composite gels are a novel strategy of formulating nanoemulsions for biomedical applications. This approach alters the way biological entities perceive and interact with the nanodroplets. The physico-chemical properties of the gel network (*i.e.*, chemical functionalization, size, shape, deformability of the particle) may be readily tuned to achieve the desired cellular interaction (*via* ligand binding, for example), circulation time, biodistribution pattern *in vivo*. The encapsulated oil droplets can be varied in size, loading and composition, depending on the 'cargo' of interest (*e.g.*, chemotherapeutic drug or imaging agent, *etc.*) and the desired release rate and delivery profile. As a drug delivery platform, nanoemulsion composites provide a promising route to achieve the targeted and systemic delivery of fragile actives.

In particular, the PFC-laden composite gels could be used during cell culture to combat diffusion limitations on oxygen and essential nutrients. Conversely, the same microparticles could be used as devices for photodynamic therapy where, in the presence of excited photosensitizers (*e.g.*, hydrophobic organic dyes), the PFC droplets act as reservoirs for the generation of singlet O_2, a cytotoxic agent known to inactivate tumor cells.[41]

Acknowledgements

H. Z. A. is supported by the Institute for Collaborative Biotechnologies through grant W911NF-09-0001 from the U.S. Army Research Office. Additional support is provided by NSF grant CMMI-1120724. The content of the information does not necessarily reflect the position or the policy of the Government, and no official endorsement should be inferred. The authors thank Nicole Billings for her help with the confocal microscopy experiments and E. P. Chang for her assistance with the light scattering and surface tension measurements. H. Z. A. thanks J. D. Mo for his helpful comments on the manuscript.

Notes and references

1 S. C. Balmert and S. R. Little, *Adv. Mater.*, 2012, **24**, 3757.
2 W. J. Duncanson, T. Lin, A. R. Abate, S. Seiffert, R. K. Shah and D. A. Weitz, *Lab Chip*, 2012, **12**, 2135.
3 J.-W. Yoo, D. J. Irvine, D. E. Discher and S. Mitragotri, *Nat. Rev. Drug Discovery*, 2011, **10**, 521.
4 Y. Geng, P. Dalhaimer, S. Cai, R. Tsai, M. Tewari, T. Minko and D. E. Discher, *Nat. Nanotechnol.*, 2007, **2**, 249.
5 R. K. Shah, H. C. Shum, A. C. Rowat, D. Lee, J. J. Agresti, A. S. Utada, L.-Y. Chu, J.-W. Kim, A. Fernandez-Nieves, C. J. Martinez and D. A. Weitz, *Mater. Today*, 2008, **11**, 18.
6 D. Dendukuri, S. S. Gu, D. C. Pregibon, T. A. Hatton and P. S. Doyle, *Lab Chip*, 2007, **7**, 818.
7 D. Dendukuri, D. C. Pregibon, J. Collins, T. A. Hatton and P. S. Doyle, *Nat. Mater.*, 2006, **5**, 365.
8 J. P. Rolland, B. W. Maynor, L. E. Euliss, A. E. Exner, G. M. Denison and J. M. DeSimone, *J. Am. Chem. Soc.*, 2005, **127**, 10096.
9 J. A. Champion, Y. K. Katare and S. Mitragotri, *Proc. Natl. Acad. Sci. U. S. A.*, 2007, **104**, 11901.
10 S. Bhaskar, J. Hitt, S.-W. L. Chang and J. Lahann, *Angew. Chem., Int. Ed.*, 2009, **48**, 4589.
11 J. A. Champion, Y. K. Katare and S. Mitragotri, *J. Controlled Release*, 2007, **121**, 3.
12 R. Haghgooie, M. Toner and P. S. Doyle, *Macromol. Rapid Commun.*, 2010, **31**, 128.
13 J. A. Champion and S. Mitragotri, *Proc. Natl. Acad. Sci. U. S. A.*, 2006, **103**, 4930.
14 T. J. Merkel, S. W. Jones, K. P. Herlihy, F. R. Kersey, A. R. Shields, M. Napier, J. C. Luft, H. Wu, W. C. Zamboni, A. Z. Wang, J. E. Bear and J. M. DeSimone, *Proc. Natl. Acad. Sci. U. S. A.*, 2011, **108**, 586.
15 S. Mitragotri and J. Lahann, *Nat. Mater.*, 2009, **8**, 15.
16 W. Wang, R. Xie, X.-J. Ju, T. Luo, L. Liu, D. A. Weitz and L.-Y. Chu, *Lab Chip*, 2011, **11**, 1587.
17 D. Jagadeesan, I. Nasimova, I. Gourevich, S. Starodubtsev and E. Kumacheva, *Macromol. Biosci.*, 2011, **11**, 889.
18 H. Z. An, M. E. Helgeson and P. S. Doyle, *Adv. Mater.*, 2012, **24**, 3838.
19 C.-H. Choi, D. A. Weitz and C.-S. Lee, *Adv. Mater.*, 2013, **25**, 2536–2541.
20 R. K. Shah, J.-W. Kim, J. J. Agresti, D. A. Weitz and L.-Y. Chu, *Soft Matter*, 2008, **4**, 2303.
21 M. E. Helgeson, S. E. Moran, H. Z. An and P. S. Doyle, *Nat. Mater.*, 2012, **11**, 344.
22 L.-Y. Chu, A. S. Utada, R. K. Shah, J.-W. Kim and D. A. Weitz, *Angew. Chem.*, 2007, **119**, 9128.
23 E. Amstad, S.-H. Kim and D. A. Weitz, *Angew. Chem., Int. Ed.*, 2012, **51**, 12499.
24 J. G. Riess, *Artif. Cells, Blood Substitutes, Biotechnol.*, 2005, **33**, 47.
25 K. C. Lowe, M. R. Davey and J. B. Power, *Trends Biotechnol.*, 1998, **16**, 272.
26 K. Chin, S. F. Khattak, S. R. Bhatia and S. C. Roberts, *Biotechnol. Prog.*, 2008, **24**, 358.
27 T. G. Mason, J. N. Wilking, K. Meleson, C. B. Chang and S. M. Graves, *J. Phys.: Condens. Matter*, 2006, **18**, R635.
28 A. Kabalnov, *J. Dispersion Sci. Technol.*, 2001, **22**, 1.
29 A. S. Kabalnov and E. D. Shchukin, *Adv. Colloid Interface Sci.*, 1992, **38**, 69.

30 J. G. Weers and B. P. E. Binks, *Mod. Aspects Emulsion Sci.*, 1998, 292–327.
31 T. Delmas, H. Piraux, A.-C. Couffin, I. Texier, F. Vinet, P. Poulin, M. E. Cates and J. Bibette, *Langmuir*, 2011, **27**, 1683.
32 J. G. Weers and R. A. Arlauskas, *Langmuir*, 1995, **11**, 474.
33 K. Meleson, S. Graves and T. G. Mason, *Soft Mater.*, 2004, **2**, 109.
34 D. Dendukuri, P. Panda, R. Haghgooie, J. M. Kim, T. A. Hatton and P. S. Doyle, *Macromolecules*, 2008, **41**, 8547.
35 W. M. Deen, *Analysis of Transport Phenomena*, 2012.
36 J. C. Maxwell, *Treatise on Electricity and Magnetism*, 1954, vol. 1.
37 C. A. Fraker, A. J. Mendez, L. Inverardi, C. Ricordi and C. L. Stabler, *Colloids Surf., B*, 2012, **98**, 26.
38 R. B. Brown and J. Audet, *J. R. Soc., Interface*, 2008, **5**, S131.
39 M. J. Rosen and J. T. Kunjappu, *Surfactants and Interfacial Phenomena*, 2012.
40 J. G. Riess, *Vox Sang.*, 1991, **61**, 225.
41 M. C. DeRosa and R. J. Crutchley, *Coord. Chem. Rev.*, 2002, **233–234**, 351.

